Adrenomedullin-RAMP2 enhances endothelial cell maturation synergically with shear stress

Yoon, Yongdae[1], Duffy, Sean[1], Kirk, Shannon[1], Promnares, Kamoltip[1], Karki, Pratap[1], Birukova, Anna A[3], Birukov, Konstantin G[1], Yuan, Yuan[1,2,*]

[1]Department of Anesthesiology, University of Maryland School of Medicine, Baltimore, MD

[2]Section of Pulmonary, Critical Care and Sleep Medicine, Department of Medicine, Yale School of Medicine, New Haven, CT

[3]Pulmonary and Critical Care Medicine, University of Maryland School of Medicine, Baltimore, MD

* Corresponding author:

Yifan Yuan: yyuan@som.umaryland.edu; yifan.yuan@yale.edu

Abstract

Diseases in pulmonary vasculature remain challenging to study due to the lack of functional ex vivo models. Paracrine signals are enriched in whole lung tissue and are critical in regulating endothelial maturation and vascular homeostasis. Previously, we employed single-cell RNA-sequencing (scRNAseq) to systematically profile ligand-receptor (L/R) interactions within the lung vascular niche. Here, we leveraged in vitro cell culture models to evaluate different paracrine signals identified from scRNAseq data and determined that adrenomedullin (ADM)-RAMP2 could improve the endothelial maturation under dynamic flow conditions. Among the top 20 soluble ligands, we found ADM has a superior effect on enhancing vascular barrier function, as evidenced by electrical cell impedance sensing (ECIS) and XperT assays. ADM also exhibited anti-inflammatory properties, decreasing ICAM1 and increasing IkBa expression in a dose-dependent manner. Interestingly, under physiological shear stress (15 dyn/cm^2), ADM synergistically enhanced the expression of the native lung aerocyte capillary (aCap) endothelial marker EDNRB, increased anti-coagulation by increasing THBD and decreasing F3 expression. This effect was completely attenuated by blocking RAMP2, a receptor of ADM. This study highlights the potential of native paracrine cues, such as ADM/RAMP2 signaling, to enhance cellular and physiological maturation in engineered vascular models.

Introduction

Pulmonary vascular disease is a growing global health concern and a significant cause of morbidity and mortality [1]. This condition is characterized by microvascular remodeling and rarefaction and is primarily attributed to pathological changes in the vascular endothelium [2]. Current in vitro systems including organ-on-chips and organoids platforms have advanced our ability to model vascular systems by incorporating differentiated or mature endothelial cells into hydrogel or PDMS-based perfused systems. These models replicate aspects of physiological flow and intercellular communication [3-6], providing valuable insights into disease mechanisms. However, these platforms fall short of replicating the complex physiology of the human lung vasculature and lack critical microenvironmental cues in the vascular niche that is essential to alveolar endothelial function, including paracrine signaling, matrix substrate components, and correct substrate stiffness. As a result, no in vitro system can recapitulate native pulmonary vascular cellular phenotypes and physiological functions over extended periods in a controlled manner.

The vascular niche in adult lungs has been studied mechanistically, mostly during development or in response to discrete injuries, such as inhalation injury or lipopolysaccharide injection. Paracrine signals including Ang1 and KGF secreted by lung mesenchymal cells are essential to protect the integrity of the lung microvascular endothelium and prevent influx of plasma and cells from the bloodstream into the alveolus/airways (reviewed in [7]). To study the cell-cell crosstalk signals during homeostatic conditions, we previously leveraged single-cell RNA-sequencing (scRNAseq) to identify cell populations in human lungs, and characterize signals coming from alveolar epithelial, mesenchymal, and immune cells that were potentially being sensed by endothelial cells [8]. We mapped putative ligand-receptor (L/R) interactions

within and between cell types and assessed the significance of these interactions using the NicheNet database [8]. We further identified a group of L/R pairs that are highly expressed in the lung vascular niche and potentially interacting with receptors expressed by vascular endothelial cells in human lungs. In this study, we will determine the impact of these identified ligands on endothelial cells and test their ability in regulating vascular cellular phenotypes and physiological functions in the in vitro vascular model systems.

The endothelium lining the blood vessels is highly sensitive to hemodynamic forces that acts at the vascular luminal surface in the direction of blood flow (reviewed in [9]). It was proposed that endothelial cells have their preferred fluid shear stress, or 'set point' [10]. Upon exposure to 16 hours of laminar shear stress ranging from 2 to 60 dynes/cm^2, human umbilical vein endothelial cells (HUVECs) aligned in the direction of the flow and anti-inflammatory and endothelial quiescence pathways were activated in the range of 10 to 20 dynes/cm^2, but cells were misaligned or oriented perpendicularly (against the flow direction), and inflammation and coagulation signaling was activated outside this range ([10] and reviewed in [11]). Here, we compared the impact of the top 20 ligands that we identified through scRNAseq, on cell-cell junction, anti-inflammatory response, anti-coagulation, and native cellular phenotypes in both static and under dynamic flow conditions at a shear stress at 15 dynes/cm^2. We determined that adrenomedullin (ADM) exerts superior effect as compared to all other identified ligands. Additionally, ADM increases anti-coagulation signals and synergistically upregulate EDNRB, a marker of aerocyte capillary endothelial cells [8,12], under shear conditions. These findings suggest that ADM plays a critical role in preserving pulmonary endothelial homeostasis and may potentially serve as a key biological cue in engineered in vitro models of the pulmonary vasculature.

Methods

Materials

Adrenomedullin (ADM, #24889) from Cayman Chemical (MI, USA); Slit homolog 2 (SLIT2, # 8616-SL) and TNF-α (# 10291-TA) from R&D Systems (MN, USA); Angiopoietin-1 (ANGPT1, #923-AN) and Bone morphogenic protein 5 (BMP5, # 615-BMC-020) from Novus Biologicals (CO, USA); and Wnt-2 (#CSB-YP026133HU, CUSABIO, TX, USA) were purchased.

Cell culture

Human pulmonary artery endothelial cells (HPAECs) were purchased from Lonza (Basel, Switzerland). The cells between passage 6-7 were placed on fibronectin 1 μg/cm^2 coated plates and were incubated in EGM-2 endothelial cell growth medium-2 bulletkit from Lonza under a cell culture incubator at 37□ with 5% CO_2 and a humidified atmosphere.

Electrical cell-substrate impedance sensing

Electrical cell-substrate impedance sensing (ECIS) assays were performed according to the manufacturer's instructions. Briefly, ECIS Cultureware plates (e.g., 96W20idf for static conditions or 1F8x10E chips for shear stress) from Ibidi (Grafelfing, Germany) were incubated with L-cysteine (10 mM) and then coated with fibronectin (1 μg/cm²). For static conditions, cells were incubated for 2 days until a stable baseline impedance was achieved. Ligands were then added to the cells, and changes in impedance were measured to determine endothelial cell permeability. For shear stress conditions, cells were incubated for 1 day after attachment. A unidirectional shear stress of 15 dyn/cm² was applied to the cells, and ADM was added for one more day with continuous impedance measurement.

Expression permeability test assay

To verify endothelial cell permeability to macromolecules, expression permeability test (Xpert) assay was performed, as previously described[13]. In brief, cells were seeded on plates coated with biotinylated collagen type I (0.25 mg/mL) dissolved in a 0.1 M bicarbonate, pH 8.3 solution. After ligand treatment, the cells were incubated with FITC-avidin (25 µg/mL) for 2 minutes. Unbound FITC-avidin was removed by washing with PBS. The fluorescence signal was then either visualized using an EVOS microscope (Thermo Fisher Scientific, MA, USA) or measured with a SpectraMax® iD5 microplate reader (Molecular Devices, CA, USA).

Western blot

Cells were lysed with 2x Laemmli sample buffer (#1610737, Bio-Rad, CA, USA). The lysates were boiled for 5 minutes and then subjected to SDS-polyacrylamide gel electrophoresis (SDS-PAGE). Proteins were transferred onto a polyvinylidene difluoride (PVDF) membrane (Bio-Rad). The membrane was blocked with 5% skim milk or 5% BSA in Tris-HCl-buffered saline containing 0.05% Tween 20 (TBST) for 30 minutes. It was then incubated with primary antibodies against ICAM-1 (sc-8439) and GAPDH (sc-47724) from Santa Cruz Biotechnology (Santa Cruz, CA, USA), as well as IκBα (#4814), NF-κB p65 (#3032), and phospho-NF-κB p65 Ser536 (#3031) from Cell Signaling Technology (MA, USA). Primary antibody incubation was performed overnight at 4°C. Following primary antibody incubation, the membrane was incubated with horseradish peroxidase (HRP)-conjugated secondary antibodies (7074S and 7076S, Cell Signaling Technology) for 2 hours. After washing the membrane three times with TBST, the protein bands were visualized using a ChemiDoc XRS+ System (Bio-Rad) after

treatment with SuperSignal West Pico PLUS or Atto Ultimate sensitivity chemiluminescent substrate (34578 or A38556, Thermo Fisher Scientific).

qPCR

Total RNA was purified using the RNeasy Plus Mini Kit (#74136, Qiagen, Hilden, Germany) according to the manufacturer's instructions. Complementary DNA (cDNA) was synthesized from the purified RNA using an iScript cDNA Synthesis Kit (#1708890, Bio-Rad). For real-time PCR, the cDNA was mixed with gene-specific primers and PerfeCta SYBR Green FastMix (Quantabio, MA, USA). The reactions were run on a CFX Opus 384 Real-Time PCR System (Bio-Rad). The primer sequences are listed in Table S1. Relative mRNA expression was quantified using the $2^{-(\Delta\Delta Ct)}$ method.

Enzyme-linked Immunosorbent Assay (ELISA)

The levels of soluble intercellular adhesion molecule-1 (ICAM-1) in the culture medium were measured using a human ICAM-1 ELISA kit (#DY720) and a Clear Microplate (#DY990) from R&D Systems (MN, USA). Cells were treated with TNF-α (1 ng/mL) for 30 minutes, followed by treatment with ADM (100 ng/mL) for 6 hours. The assay was performed according to the manufacturer’s instructions. The values were quantified by measuring absorbance at 450 nm using a SpectraMax® iD5 (Molecular Devices, CA, USA).

Shear Stress

To apply a unidirectional shear stress to endothelial cells, we utilized an ibidi pump system (#10902, ibidi, Gräfelfing, Germany). The cells were seeded on µ-Slide 0.4 Luer ibiTreat

(#80176, Ibidi) coated with fibronectin (1–2 μg/cm²). Following the manufacturer's instructions, the slides were connected to the pump system. The cells were subjected to either 5 or 15 dyne/cm² shear stress for 1 day. Subsequently, the medium was carefully replaced with fresh medium and ADM (100 ng/ml) added ADM, and the cells were incubated for an additional day under continuous shear stress.

Immunofluorescence

For static condition, HPAECs seeded in glass coverslips which were coated with fibronectin 2 μg/cm^2. For shear stress condition, the cells were seeded in a μ-Slide $^{0.4}$ Luer ibiTreat chip (#80176, Ibidi) with fibronectin coating. Both cells were fixed with 2% paraformaldehyde in PBS including Ca^{2+} and Mg^{2+} and permeabilized with 0.1% Triton X-100 in PBS for 15 min at RT. Following a 30 min block with 5% BSA in PBS, the cells were incubated with VE-cadherin antibody (#93467, Cell Signaling Technology) in 5% BSA in PBS at 4 °C overnight. The cells were then labeled by an Alexa Fluor™ Plus 488-conjugated secondary antibody (Invitrogen, CA, USA) for 1h at RT. For filamentous actin staining, the cells were incubated with Texas Red-X phalloidin (#T7471, Thermo Fisher Scientific) for 30 min at RT. After DAPI staining (#62248, Thermo Fisher Scientific), the stained cells were mounted by a ProLong glass antifade Mountant. Images were captured using a fluorescent microscope (Eclipse TS2R, Nikon, Tokyo, Japan).

siRNA transfection

Transfection of RAMP2 (sc-36378) or control siRNA (sc-37007) from Santa Cruz Biotechnology (Santa Cruz, CA, USA) was performed using Lipofectamine RNAiMAX Transfection Reagent (13778-075, Thermo Fisher Scientific, MA, USA) according to the

manufacturer's instructions. Briefly, HPAECs were seeded in fibronectin (1 µg/cm²)-coated 6-well plates. The cells were then transfected with either RAMP2 or control siRNA. Following a 24-hour incubation, the transfected cells were replated onto ECIS plates for static conditions, ECIS chips for shear stress experiments, or µ-Slide Luer ibiTreat chips for immunofluorescence.

Statistical analysis

Data are presented as the mean ± standard deviation (SD) from three independent experiments. Statistical analysis was performed using GraphPad Prism 10 software. Differences between two groups were analyzed with an unpaired Student's t-test. A p-value of less than 0.05 was considered statistically significant. *$p<0.05$; **$p<0.01$; and ***$p<0.001$

Results

ADM exerts improving lung endothelial cell barrier function and anti-inflammatory effects by TNF-α

To understand the factors that regulate the microvascular environment, we screened for soluble factors released by alveolar epithelial, mesenchymal, and immune cells within the microvascular niches that could interact with receptors on alveolar endothelial cells (Figure 1A and [8]). Among the screened ligands, both adrenomedullin (ADM) and angiopoietin1 (ANGPT1) enhanced endothelial cell barrier integrity and ADM showed the strongest effect in human pulmonary endothelial cells (HPAECs). In contrast, vascular endothelial growth factor A (VEGFA) and several inflammatory cytokines such as CXCL6, CCL19, and BMP5, impaired the barrier (Figure 1B). Furthermore, ADM increased barrier function in a dose- dependent manner at concentration between 10 to 100 ng/ml in HPAECs (Figure 1C). In addition, endothelial cell

permeability to macromolecules was measured using expression permeability test (Xpert). In agreement with the results of barrier function assay conducted by electrical cell-substrate impedance sensing (ECIS), ADM inhibited infiltration of macromolecules in a dose-dependent manner (Figure 1D).

Inflammatory is a major factor that impair vascular integrity, and its inhibition is essential for maintaining a healthy environment integrity. Therefore, we investigated the anti-inflammatory effects of ADM. ADM significantly decreased the TNF-α-induced ICAM-1, a protein involved in the recruitment of immune cells to inflammatory sites. Furthermore, ADM restored the TNF-α-induced degradation of IκBα, which inhibits the NF-κB signaling pathway (Figure 2A and B). These anti-inflammatory effects are consistent with the ADM-induced vascular integrity regulation observed at 10 and 100 ng/ml (Figure 1). Likewise, ADM inhibited the TNF-α-induced secretion of ICAM-1 (Figure 2E). In addition, ADM also reduced the phosphorylation of p65, a subunit of NF-κB (Figure 2C and D). Therefore, these results indicate that ADM enhances vascular integrity and exhibits anti-inflammatory responses.

ADM exhibits synergistic effect in maintaining alveolar endothelial integrity under mechanical force.

Pulmonary endothelial cells are exposed to a unique variety of mechanical forces, such as shear stress from blood flow and stretching from respiration. To induce shear stress on endothelial cells, we utilized an ibidi pump system to produce unidirectional flow at 5 or 15 dynes/cm^2. Under shear stress, mechanosensory genes such as KLF2 and KLF4 as well as pan-endothelial genes such as CD31, CDH5, and eNOS increased in HPAECs. In contrast, the expression of CLDN5, highly expressed in lung and brain endothelial cells, was decreased (Figure 3A and B).

Although shear stress at 5 dynes/cm^2 had a weaker effect on gene expression levels, the patterns were consistent with the results from the higher shear stress condition (data not shown). ADM still had enhancing endothelial cell integrity under shear stress condition (Figure 3C). Immunofluorescence images showed that shear stress changed cell morphology and reorganized F-actin filaments in the direction of flow. In contrast, the cells in static condition were randomly oriented, with F-actin filaments located along the cell borders where they associate with VE-cadherin (Figure 3D). Although F-actin filaments and cell morphology were altered under shear stress condition, the cells adapted to the environment, maintaining similar cell-cell junctions and VE-cadherin expression compared to static conditions (Figure 3D). Furthermore, ADM treatment reorganized VE-cadherin along the cell borders, promoting a more linear and thicker arrangement that led to the structural reinforcement and stabilization of cell-cell junctions in both static and shear stress conditions (Figure 3D). Interestingly, a number of receptors involved in endothelial cell regulation were upregulated under shear stress. Among these, RAMP2, a specific co-receptor for ADM, was the most highly expressed. Notably, ADM treatment did not alter the expression of either RAMP2 or CALCRL (Figure 3E). The calcitonin receptor-like receptor (CALCRL) is a unique signaling receptor that forms a complex with receptor activity modifying proteins (RAMPs). This interaction is critical as the specific RAMP bound to CALCRL determines its affinity for either adrenomedullin (ADM) or calcitonin gene-related peptide (CGRP). Next, we found that shear stress increased the aerocyte specific marker gene, EDNRB. ADM treatment further enhanced this gene's expression, while having no effect on the expression of SOX17, an arterial marker, or ACKR1, a vein marker (Figure 3F). Although we attempted to detect general capillary endothelial cell marker gene, CD36, HPAECs did not express this gene under either static or shear stress condition (data not shown). Shear stress also

modulated the expression of coagulation-related genes, such as coagulation factor III (F3), a marker for coagulation, and thrombomodulin (THBD), a marker for anti-coagulation (Figure 3G). This suggests that shear stress may regulate a balance between pro- and anti-coagulant states. Notably, ADM treatment shifted the balance toward an anti-coagulation status by decreasing F3 but increasing THBD (Figure 3G). These gene expression regulation also had happened at the lower shear stress condition, although the levels were less pronounced than at the higher speed (data not shown). Hence, these results suggest that while shear stress helps maintain endothelial cell character, ADM further drives the cells toward a pulmonary capillary endothelial cell (aerocyte) identity and a more pronounced anti-coagulation state.

Endothelial cell functions induced by ADM are regulated by RAMP2 signaling pathway

Given that shear stress increased RAMP2 expression and that ADM had significant effects on maintaining endothelial cell character and anti-coagulation, we hypothesized that the effects of ADM may be mediated by RAMP2. Therefore, we investigated the effects of ADM after RAMP2 was knocked down with siRNA to determine if its regulatory effects are dependent on RAMP2. The ability of ADM to enhance endothelial cell barrier function was hampered in both static and shear stress conditions following siRNA-mediated knockdown of RAMP2 (Figure 4A and B). Furthermore, the ADM-induced linear and thicker arrangement of VE-cadherin along the cell borders was also eliminated after RAMP2 knockdown (Figure 4C). Ultimately, the regulation of EDNRB, F3, and THBD gene expression by ADM under shear stress was eliminated in RAMP2 knockdown cells (Figure 4D). Thus, these data demonstrate that ADM-induced effects on barrier function are dependent on RAMP2 expression. They further suggest that baseline RAMP2 levels are not sufficient to elicit a response to ADM under static condition.

Discussion

In this study, we determined that ADM exerts a superior impact on barrier enhancement in human lung endothelial cells as compared to other ligands tested. We further showed that the treatment with ADM reduces inflammatory responses to TNF-α. Under physiological flow conditions, treatment with ADM maintains its function to improve vascular barrier function, and further exerts anti-coagulation effect and improves native cellular characteristics. Therefore, paracrine signals identified from native vascular niche, such as ADM, might contribute to homeostasis in the in vitro vascular model system, and this favorable impact may not be limited to just vascular engineering alone.

Leveraging scRNAseq, we previously identified a group of ligand-receptor pairs that are enriched in the vascular niche in the healthy adult human lungs [8]. However, the impact of these factors on endothelial cell behaviors has not been studied. In the current study, we applied two different assays (ECIS and XperT) to compare the effects of different ligands on endothelial cell barrier function. Our data confirmed that Ang-1 and ADM significantly decreased endothelial permeability in both assays, consistent with previous literature[14,15]. Interestingly, we observed that the ADM had significantly increased function in improving the vascular barrier as compared to other molecules, which prompts us to focus on ADM in further studies.

Figure Captions

Figure 1. ADM exhibits superior effect on enhancing vascular barrier function. (A) The image presents an overview of experimental flow, including a list of candidate ligands that were

selected from a preliminary analysis of ligand/receptor pair between endothelial cells and non-endothelial cells in macrovascular environments. (B) HPAECs' barrier function was tested by ECIS assay after the cells were treated with the selected 16 ligands. (C) Different concentrations of ADM, from 1 to 100 ng/ml, were treated to HPAECs, and the regulating barrier function was measured using ECIS assay. (D) HPAECs were seeded on biotinylated collagen type I (0.25 mg/mL) coated well plates. The cells were pretreated with the indicated ADM concentrations for 1 hour, and FITC-conjugated avidin was added for 2 minutes. The FITC fluorescence was measured, and the image of FITC signal was captured after DAPI staining. The graph is presented as the means ± standard deviation (SD) from three independent experiments. **$p<0.01$

Figure 2. ADM reduces pro-inflammatory responses against TNF-α. (A and C) HPAECs were treated with 1 ng/ml TNF-α for 30 minutes, followed by the indicated concentrations of ADM for 5.5 hours. The samples were subjected to Western blot (WB) analysis to detect ICAM-1, IκBα, Phosphorylated-p65, total p65, and GAPDH proteins. (B) ICAM-1 and IκBα proteins were normalized to GAPDH, and the values were presented as a bar graph. (D) Phosphorylated-p65 expression was normalized to total p65 protein levels. (E) The cultured medium from cells treated with 1 ng/ml TNF-α for 30 minutes, followed by AND for 5.5 hours, was used to measure soluble ICAM-1 expression levels by ELISA assay. The graphs are presented as the means ± standard deviation (SD) from three independent experiments. *$p<0.05$ and **$p<0.01$

Figure 3. ADM synergistically improves endothelial characteristics with physiological shear stress. (A and B) HPAECs were incubated under unidirectional flow at 15 dyne/cm^2 for 1 day. The expressions of mechanosensory genes (KLF2 and KLF4) and pan-endothelial cell marker genes (CD31, CLDN5, CDH5, and eNOS) were amplificated by real time PCR, normalized to GAPDH, and presented as graphs. (C) The cell barrier function was measured by ECIS assay.

The graph shows the results from the cells treated with 100 ng/ml ADM after 1 day of shear stress at 15 dyne/cm^2. (D) The fluorescence images were taken after the cells were treated with 100 ng/ml of ADM for 1 hour under both static and shear stress conditions. For shear stress condition, the cells were incubated for 1day at 15 dyne/cm^2 before the ADM treatment. (E-G) The cells were incubated with either static or shear stress condition for 1 day, and then 100 ng/ml of ADM was added to the cells after medium change for 30 minutes. The indicated gene expressions were measured by real-time PCR and normalized to GAPDH. The graphs are presented as the means ± standard deviation (SD) from three independent experiments. *****$p<0.05$, ******$p<0.01$, and *******$p<0.001$

Figure 4. Knockdown of RAMP2 attenuates the response of improved phenotype by ADM. To knock down of RAMP2 gene expression, control or RAMP2 siRNA (10 nM) were transfected into HPAECs. The ability of ADM (100 ng/ml) to enhance endothelial cell barrier function was measured under both (A) static and (B) shear stress (15 dyne/cm^2) conditions. (C) The fluorescence images captured from the cells treated with ADM (100 ng/ml) for 1 hour, under both static and shear stress (15 dyne/cm^2) conditions after transfection of control or RAMP2 siRNA. (D) The genes EDNRB, F3, and THBD, which are regulated by ADM treatment under shear stress, were assessed in the RAMP2 knockdown condition. The graphs are presented as the means ± standard deviation (SD) from three independent experiments. *****$p<0.05$ and ******$p<0.01$

References

1. Ejikeme C, Safdar Z. Exploring the pathogenesis of pulmonary vascular disease. Front Med (Lausanne) 2024;11:1402639. DOI: 10.3389/fmed.2024.1402639.
2. Huertas A, Guignabert C, Barbera JA, et al. Pulmonary vascular endothelium: the orchestra conductor in respiratory diseases: Highlights from basic research to therapy. Eur Respir J 2018;51(4). DOI: 10.1183/13993003.00745-2017.

3. Qiu Y, Lin J, Wang A, et al. Clinically relevant clot resolution via a thromboinflammation-on-a-chip. Nature 2025;641(8065):1298-1308. DOI: 10.1038/s41586-025-08804-7.
4. Qiu Y, Ahn B, Sakurai Y, et al. Microvasculature-on-a-chip for the long-term study of endothelial barrier dysfunction and microvascular obstruction in disease. Nat Biomed Eng 2018;2:453-463. DOI: 10.1038/s41551-018-0224-z.
5. Wimmer RA, Leopoldi A, Aichinger M, et al. Human blood vessel organoids as a model of diabetic vasculopathy. Nature 2019;565(7740):505-510. DOI: 10.1038/s41586-018-0858-8.
6. Miao Y, Pek NM, Tan C, et al. Co-development of mesoderm and endoderm enables organotypic vascularization in lung and gut organoids. Cell 2025;188(16):4295-4313 e27. DOI: 10.1016/j.cell.2025.05.041.
7. Wettschureck N, Strilic B, Offermanns S. Passing the Vascular Barrier: Endothelial Signaling Processes Controlling Extravasation. Physiol Rev 2019;99(3):1467-1525. DOI: 10.1152/physrev.00037.2018.
8. Schupp JC, Adams TS, Cosme C, Jr., et al. Integrated Single-Cell Atlas of Endothelial Cells of the Human Lung. Circulation 2021;144(4):286-302. DOI: 10.1161/CIRCULATIONAHA.120.052318.
9. Davies PF. Hemodynamic shear stress and the endothelium in cardiovascular pathophysiology. Nat Clin Pract Cardiovasc Med 2009;6(1):16-26. DOI: 10.1038/ncpcardio1397.
10. Baeyens N, Nicoli S, Coon BG, et al. Vascular remodeling is governed by a VEGFR3-dependent fluid shear stress set point. Elife 2015;4. DOI: 10.7554/eLife.04645.
11. Cheng CK, Wang N, Wang L, Huang Y. Biophysical and Biochemical Roles of Shear Stress on Endothelium: A Revisit and New Insights. Circ Res 2025;136(7):752-772. DOI: 10.1161/CIRCRESAHA.124.325685.
12. Gillich A, Zhang F, Farmer CG, et al. Capillary cell-type specialization in the alveolus. Nature 2020;586(7831):785-789. DOI: 10.1038/s41586-020-2822-7.
13. Birukova AA, Shah AS, Tian Y, Moldobaeva N, Birukov KG. Dual role of vinculin in barrier-disruptive and barrier-enhancing endothelial cell responses. Cell Signal 2016;28(6):541-51. DOI: 10.1016/j.cellsig.2016.02.015.
14. Muller HC, Witzenrath M, Tschernig T, et al. Adrenomedullin attenuates ventilator-induced lung injury in mice. Thorax 2010;65(12):1077-84. DOI: 10.1136/thx.2010.135996.
15. Gutbier B, Neuhauss AK, Reppe K, et al. Prognostic and Pathogenic Role of Angiopoietin-1 and -2 in Pneumonia. Am J Respir Crit Care Med 2018;198(2):220-231. DOI: 10.1164/rccm.201708-1733OC.

Figure 1 – ADM exhibits superior effect on enhancing vascular barrier function

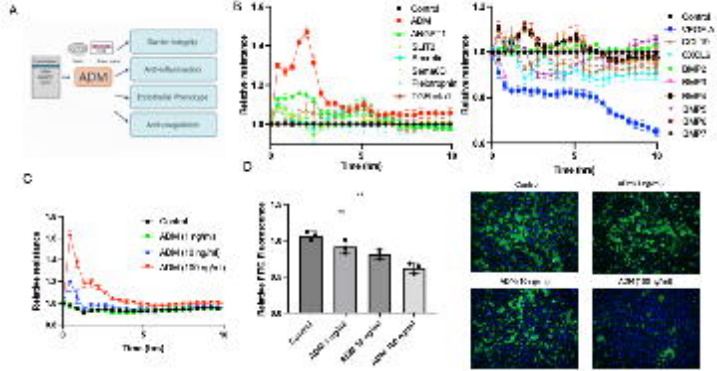

Figure 2 – ADM reduces pro-inflammatory responses against TNF

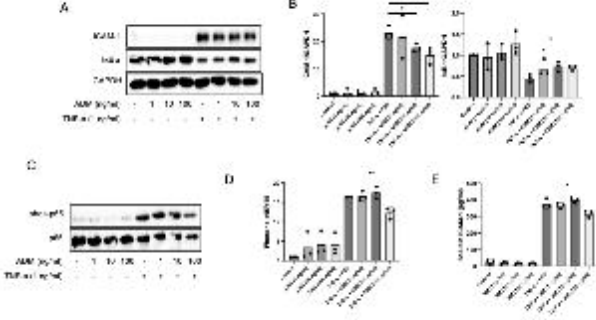

Figure 3 – ADM synergistically improves endothelial characteristics with physiological shear stress

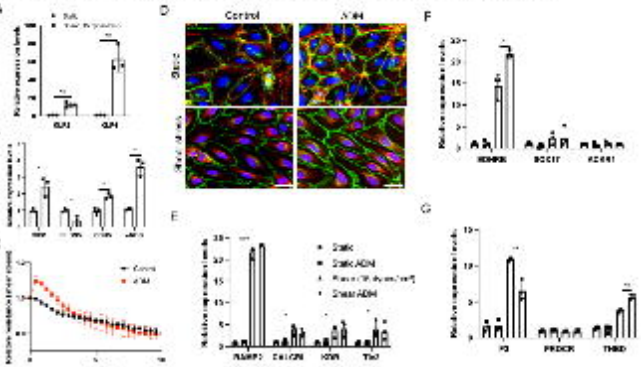
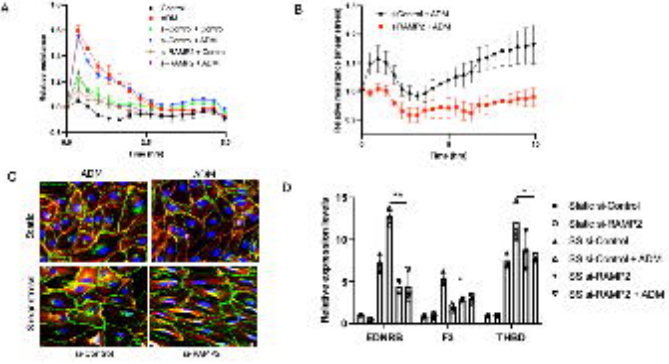
Figure 4 – Knockdown of RAMP2 attenuates the response of improved phenotype by ADM